IL NUOVO CIMENTO **48 C** (2025) 44
DOI 10.1393/ncc/i2025-25044-y

COLLOQUIA: IWM-EC 2024

Quantifying neutron-proton equilibration using molecular dynamics codes

A. JEDELE(1)(2)(*), K. HAGEL(1), M. Q. SORENSEN(1)(2), B. HARVEY(1)(3), A. ABBOTT(1)(2), J. GAUTHIER(1), A. HANNAMAN(1)(2), A. A. HOOD(1), Y.-W. LUI(1), L. MCCANN(1)(2), A. B. MCINTOSH(1), L. A. MCINTOSH(1), S. SCHULTZ(1)(2), Z. TOBIN(1)(2), R. WADA(1), M. YOUNGS(1) and S. YENNELLO(1)(2)(3)

(1) *Cyclotron Institute, Texas A&M University - College Station, TX, USA*
(2) *Chemistry Department, Texas A&M University - College Station, TX, USA*
(3) *Physics Department, Texas A&M University - College Station, TX, USA*

received 26 November 2024

Summary. — Previous studies have quantified neutron-proton equilibration experimentally in dynamically deformed nuclei in heavy ion collisions (JEDELE A. *et al.*, *Phys. Rev. Lett.*, **118** (2017) 062501; RODRIGUEZ MANSO A. *et al.*, *Phys. Rev. C*, **95** (2017) 044604). The results showed the composition of the two heaviest fragments from the excited projectile-like fragment evolve exponentially with respect to its angle of rotation. Simulations using constrained molecular dynamics and antisymmetrized molecular dynamics were utilized for different slope parameterizations to compare the experimental results. The results indicate better agreement with a softer interaction.

1. – Introduction

Neutron-proton equilibration can give insight into the density dependence of the asymmetry term of the nuclear equation of state (nEoS). In peripheral and mid-peripheral collisions, a low density neck region forms between the projectile and target, characterized as being relatively neutron-rich. The extent of the neutron flow is governed by the form of the density dependence of the nEoS. Due to a velocity gradient, the system becomes highly elongated before breaking apart into an excited projectile-like fragment (PLF*) and excited target-like fragment (TLF*). Focus was placed on the PLF* due to detection

(*) Present address: Institute für Kernphysik, Technische Universität Darmstadt - Darmstadt, Germany; Gesellschaft für Schwerionenforschung - Darmstadt, Germany.

limitations. The PLF* continues to rotate around its center-of-mass eventually breaking apart into a second heaviest fragment (LF) and heaviest fragment (HF).

The PLF* decays either via statistical or dynamical decay. In dynamical decay, the fragments break apart along the TLF-PLF axis of separation due to high deformation and elongation of the PLF*. The PLF* break apart on a very short timescale of 10^{-21} s and ordered relative to size, where the HF decays forward of the LF. Statistical decay occurs when the surface tension is large enough to form a spherical PLF* followed by isotropical decay on a longer timescale (10^{-20}–10^{-19} s).

The HF and LF regions have different chemical potentials leading to neutron and proton flow to minimize the difference, known as neutron-proton (NZ) equilibration. The extent of the NZ equilibration is determined by the contact time. For dynamical decay, since the contact time is very short, the LF is relatively neutron-rich and the HF is relatively neutron-poor. Statistically decaying fragments should achieve equilibrium before breaking apart.

Previous experimental results [1, 2] quantified the NZ equilibration as exponential in nature with an average rate constant of 0.3 zs for both the HF and LF. Further insight into the functional form of the density dependence of the nEoS can be gained by comparing the results to simulations.

2. – Experimental and simulation conditions

Experimentally, symmetric reaction of ^{70}Zn+^{70}Zn at 35 MeV/nuc. were performed at the Cyclotron Institute at Texas A&M University using the K500 cyclotron. The results were obtained using the Neutron and Ion Multidetector-array for Reaction Oriented Dynamics (NIMROD) [3], as the array has isotopic identification up to $Z = 17$ in many detectors and $Z = 20$ in select Si-Si-CsI telescopes [4]. Elemental identification is achieved to $Z = 30$. Additionally, NIMROD has a large angular coverage of 3.6°–167.0°.

COnstrained Molecular Dynamics (COMD) [5] and Anti-symmetrized Molecular Dynamics (AMD) [6] codes were run. These molecular dynamics codes simulate the reaction dynamics by solving time-dependent wave functions. In both cases, Pauli exclusion principle is preserved. In the case of AMD, it is conserved through solving anti-symmetrized Slater determinants, and in the case of COMD, it is preserved using occupational densities. The parameterization of the density dependence of the nEoS comes from a Skyrme interaction.

An order of magnitude of 10^7 events were simulated for each asymmetry energy parameter for COMD. The input parameters extracted correspond to slopes of $L = 51$ MeV, $L = 75$ MeV and $L = 105$ MeV for the soft interaction, stiff and super-stiff interaction, respectively. In all three cases, the saturation energy corresponded to $E_{sym}(\rho_0) = 30$ MeV/nuc. The simulation was stopped at 1000 fm/c, corresponding to when previous work had shown the majority of dynamical decay had occurred [7]. A triangular distribution was used for the impact parameter.

An order of magnitude of 10^5 events were simulated for each asymmetry energy parameter for AMD. The input parameters extracted correspond to slopes of $L = 21$ MeV and $L = 65$ MeV for the soft interaction and stiff interaction, respectively. In all three cases, the saturation energy corresponded to $E_{sym}(\rho_0) = 30.5$ MeV/nuc. The simulation was stopped at 300 fm/c, corresponding to a compromise between CPU time and complete dynamical decay. A mixture of uniform and triangular distributions for the impact

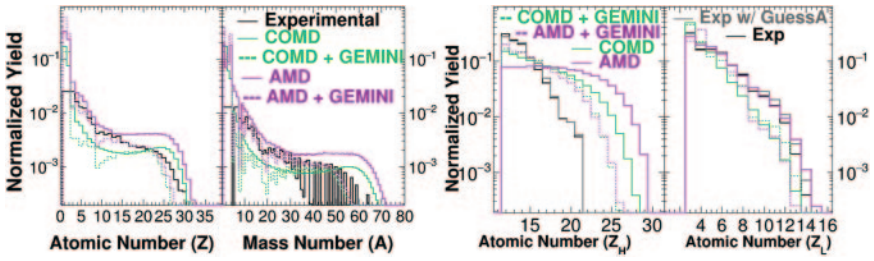

Fig. 1. – In the left panel, charge and mass distributions. The experimental results are plotted in black. The COMD results are in teal and the AMD results are in purple. The solid lines correspond to the non-de-excited results, and the dotted lines correspond to the results with GEMINI. The zigzag effect in the mass distribution is due to the isotopic resolution of NIMROD. In the right panel, charge distributions of Z_H and Z_L. The coloring is consistent with the figure of the left panel. The grey distributions are experimental distributions, where the isotopic requirement is removed.

parameter was used (5% and 95%, respectively, for the soft interaction, and 8% and 92%, respectively, for the stiff interaction).

For both simulations, output from the simulation was directly passed through a software replica of the NIMROD filter to reproduce the experimental parameters. The same output was also passed through the GEMINI [8] de-excitation code to simulate effects due to secondary decay before passing through the NIMROD filter. The results for the charge and mass distributions are shown in fig. 1 (left panel). The black lines correspond to the experimental data. The teal lines are the COMD results and the purple lines are the AMD results. The simulation results without GEMINI are plotted with solid lines and the results without are plotted with dotted lines. All distributions are normalized relative to the total yield. The zigzag effect in the experimental-mass distribution is due to the isotopic identification limitations for $Z > 17$. For fragments that are elementally identified, but not isotopically, a GuessA value is assigned. In the case of both simulations, greater agreement with the experimental values for both the mass and charge distributions is seen for the results with GEMINI.

Event selections were applied in order to focus on dynamically decaying events. All fragments passing through the filter were sorted by charge, followed by mass and then velocity. The largest fragment was labelled HF and required to have a charge of $Z_H \geq 12$. The second largest fragment was labelled LF and had a charge requirement of $Z_L \geq 3$. The distribution is plotted in fig. 1 (right panel). All fragments had to be isotopically identified.

Next, the velocity distributions were compared to give insight into the origin of the fragments. Both the $\langle v_H \rangle$ and $\langle v_L \rangle$ are greater than mid-velocity, indicating the fragments originate from the PLF*. The fragments are ordered with $\langle v_H \rangle > \langle v_L \rangle$, consistent with decay on a very short timescale. The $\langle v_H \rangle$ maintains a velocity similar to the beam velocity, whereas the $\langle v_L \rangle$ constitutes an origin from the neck. The combination indicates prompt decay along the axis of separation, consistent with previous results [9-11]. With the exception of the COMD v_H distribution, the simulated results are lower than the experimental ones, indicating over-interaction.

3. – Angular distributions

Further reaction information can be obtained by examining the rotation angle, which is defined as the dot product of the center-of-mass and relative velocity (eq. (1)),

$$\alpha = \mathrm{acos}\left(\frac{\vec{v}_{CM}\cdot\vec{v}_{REL}}{||\vec{v}_{CM}||||\vec{v}_{REL}||}\right). \tag{1}$$

The left panel of fig. 2 shows the $\cos(\alpha)$ distribution for the experimental and simulated results. The colors and line styles are consistent with fig. 1. A large peak at $\cos(\alpha) = 1$ constitutes dynamical decay, where the HF is emitted forward relative to the LF. In peripheral and mid-peripheral reactions, the highly deformed PLF* will most likely break apart quickly along the PLF-TLF axis of separation due to a large velocity gradient. The longer the PLF* staying in contact, the more it rotates around its center-of-mass until most likely breaking apart, resulting in a smaller $\cos(\alpha)$ value. The trend is noted in the left panel of fig. 2, where the $\cos(\alpha)$ distribution falls off fairly quickly, becoming constant at $-1 \leq \cos(\alpha) \leq -0.3$, consistent with statistical decay.

One interesting feature of the left panel of fig. 2 is the significant decrease in the peak at $\cos(\alpha) = 1$ and increase of yield around $-1 \leq \cos(\alpha) \leq -0.3$ for the COMD simulations when GEMINI is applied. Upon further inspection, the source comes from whether the PLF* decayed into a HF and LF by the end of the COMD simulation time. Events where the fragments had decayed before applying GEMINI are most likely produced dynamically and will be referred to as different source events throughout the analysis. If an event has not decayed into a HF and LF by the end of the simulation, GEMINI does not preserve the reaction dynamics, resulting in statistically decayed fragments. These events are referred to as same source events. The right panel of fig. 2 shows the COMD and AMD same and different source breakdown relative to the total distribution. In COMD, 69% of events originate from a same source in comparison to 25% in the case of AMD. Throughout the remainder of the publication, only different source events are analysed when looking at GEMINI results.

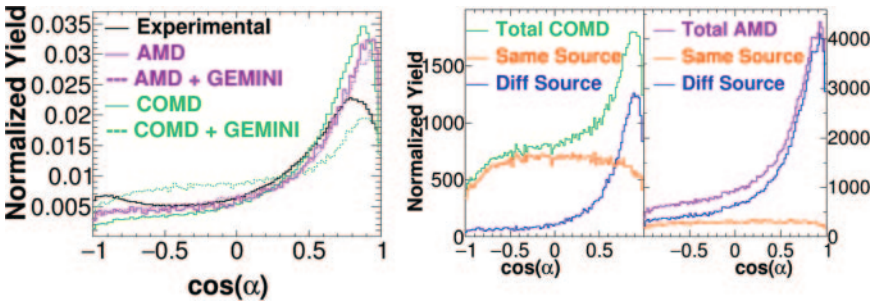

Fig. 2. – In the left panel $\cos(\alpha)$ distribution for simulated and experimental results. Colors are consistent with fig. 1. Large yield at $\cos(\alpha)$=1 is consistent with dynamical decay. In the right panel $\cos(\alpha)$ distribution broken down based on whether the PLF* decayed before (orange line) or (blue line) after GEMINI was applied.

4. – NZ equilibration results

The composition of the HF and LF were calculated using the formula $\Delta = \frac{N-Z}{A}$. In comparison to the work from ref. [1], the statistics were lacking to quantify the $\langle\Delta_H\rangle$ and $\langle\Delta_L\rangle$ as a function of both Z_H and Z_L. Due to this, when calculating $\langle\Delta_H\rangle$, a cut was made on Z_H, but not on Z_L, and vice versa for Δ_L. The results were compared for the three different slope parameterizations (soft, stiff and super-stiff) for COMD and the two parameterizations (soft and stiff) for AMD.

Focusing first on the COMD results, the results for the soft interaction were plotted in fig. 3. The left panels correspond to the $\langle\Delta_L\rangle$ as a function of α, and the right panels correspond to the Δ_H as a function of α. The ordering from top to bottom is COMD with GEMINI, COMD without GEMINI and the experimental results from refs. [1, 2], respectively. The coloring in each of the left panels is consistent and covers a range from $3 \leq Z_L \leq 9$. The range for the right-hand panel is $13 \leq Z_H \leq 18$ and the coloring is also consistent across the right panels. The y-axis of each panel on the left and right side are equivalent.

When looking at the Δ_L *vs.* α results for all three panels, the composition starts off relatively neutron-rich, evolving exponentially to be less neutron-rich, plateauing around $\alpha \simeq 100°$. The extent of the equilibration ($|\langle\Delta_{final,L}\rangle - \langle\Delta_{init,L}\rangle|$) varies, with the greatest effect seen in the COMD without GEMINI results. The smallest difference between $\langle\Delta_{init,L}\rangle$ and $\langle\Delta_{final,L}\rangle$ is observed in the COMD results with GEMINI. The $\langle\Delta_{init,L}\rangle$ also varies, where the COMD without GEMINI shows clustering around $\langle\Delta_{init,L}\rangle = 0.1$, which is most likely an effect of the code. The COMD with GEMINI underpredicts the $\langle\Delta_{init,L}\rangle$ relative to the experimental results.

In the case of the HF, the COMD results without GEMINI overpredict the initial compositions of all Z_H. The composition increases slightly initially before plateauing between $50° < \alpha < 100°$ and then rising again at $\alpha > 100°$, not following the trend seen in the experimental data. After GEMINI is applied, the distribution flattens, washing out the characteristics seen in the upper panel. The $\langle\Delta_{init,H}\rangle$ for each charge is more consistent for the results with GEMINI compared to the experimental $\langle\Delta_{init,H}\rangle$.

To compare the three different slope parameterizations, the compositions for $5 \leq Z_L \leq 7$ and $12 \leq Z_H \leq 14$ were plotted in the left and right parts, respectively, of fig. 4 for the COMD results without GEMINI. The coloring represents different interactions,

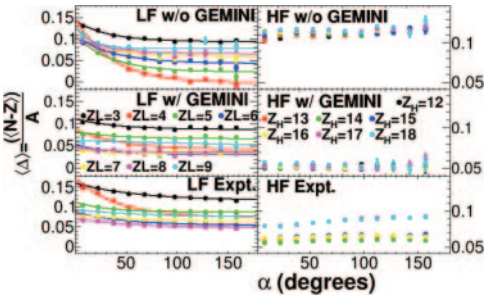

Fig. 3. – $\langle\Delta\rangle$ *vs.* α for the COMD soft interaction. Left panels correspond to Δ_L and the right panels correspond to $\langle\Delta_H\rangle$. The top panel is the COMD results without GEMINI, the middle panels show the COMD results with GEMINI, and the bottom panel is the experimental results from ref. [1,2]. The coloring is consistent for each of the left panels and each of the right panels.

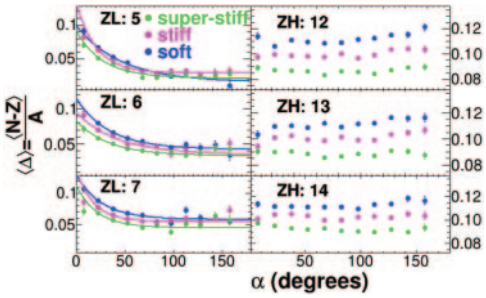

Fig. 4. – $\langle\Delta\rangle$ and *vs.* α for the soft (blue), stiff (pink) and super-stiff (green) interactions. The left part corresponds to Δ_L, ranging from $5 \leq Z_L \leq 7$, and the right part corresponds to Δ_H, ranging from $12 \leq Z_H \leq 14$.

where blue corresponds to the soft interaction, pink corresponds to the stiff one, and green corresponds to the super-stiff one.

The general trend for the Z_L is consistent with $\langle\Delta_H\rangle$ evolving exponentially to be less neutron-rich. The composition is ordered, where the the softest interaction is the most neutron-rich. Since the asymmetry energy below saturation density is greatest for a stiff interaction, the neutron flow should be the greatest, leading to a less neutron-rich composition of the LF.

For the HF, less consistency is seen amongst the interactions. An overall increase in $\langle\Delta_H\rangle$ is present for the soft interaction. This effect lessens as the interaction stiffens to the extent that the super-stiff interaction shows no increase, but rather a mostly constant composition. The composition ordering of the interactions is equivalent to the LF. In a bimodal picture of NZ equilibration, the neutron flow should be between the HF and LF, meaning that the ordering should be opposite rather than equivalent.

In order to compare the COMD, AMD and experimental results, all Z_H and Z_L combinations were combined. Figure 5 (left) shows the results for the COMD simulations and fig. 5 (right) shows the results for the AMD simulations. The filled points correspond

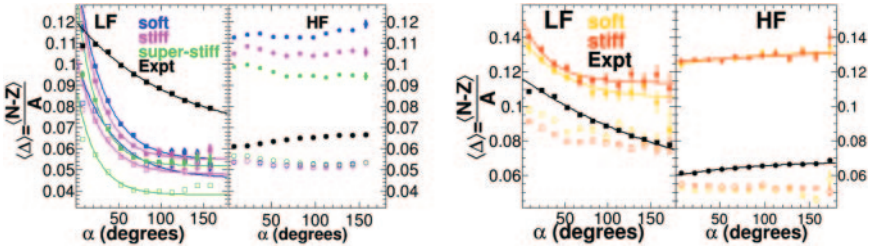

Fig. 5. – On the left, Δ *vs.* α for the soft (blue), stiff (pink) and super-stiff (green) COMD interactions and the experimental (black) results. All Z_H and Z_L values were combined. The left panel shows the LF values and the right panel shows the HF value. The filled points correspond to COMD results without GEMINI, and the open ones correspond to the COMD results with GEMINI. On the right, Δ *vs.* α for the soft (yellow) and stiff (red) AMD interactions and the experimental (black) results. All Z_H and Z_L values were combined. The left panel shows the LF values and the right panel shows the HF value. The filled points correspond to AMD results without GEMINI, and the open ones correspond to the AMD results with GEMINI.

to the results without GEMINI. In both figures, the black points correspond to the experimental data.

In the COMD simulations, the LF shows an exponential decrease with the composition reaching a plateau around $\alpha = 100°$. This is in contrast with the experimental results, where the asymptotic value is not approached by $\alpha = 180°$. For the HF, the initial composition for all three interactions without GEMINI is overpredicted. The soft interaction shows an overall increase in the composition. However, this trend is more S-shaped than the experimentally determined exponential increase. The stiff interaction shows a constant S-shaped trend, and the super-stiff interaction shows an overall decrease. When GEMINI is applied, while the $\langle\Delta_{init,H}\rangle$ is more consistent with the experimental data, the interactions show a decrease in the composition between $0° \leq \alpha \leq 120°$.

For AMD, the LF for both interactions shows an exponential evolution to a more neutron-poor configuration. The stiff interaction approaches the asymptotic value much faster than the soft interaction. Both cases overpredict the neutron richness of the LF. When GEMINI is applied, the initial composition decreases below the experimental value. The composition decreases at $\alpha \leq 60°$, before rising between $60° \leq \alpha \leq 100°$ and decreasing again at $\alpha \geq 180°$. For the HF, the $\langle\Delta_{init,H}\rangle$ is overpredicted as well. There is an overall increase in the composition of the HF. The extent of the equilibration is greatest for the soft interaction. However, in both cases, it is lower than the experimental value. After applying GEMINI, the increasing trend is completely washed out, leaving a constant distribution. The $\langle\Delta_{init,H}\rangle$ is closer to the experimental compositions. In the case of AMD and COMD simulations, the input angular momentum and excitation energy is most likely too large causing GEMINI to over-de-excite the fragments, washing out the reaction dynamics signature.

5. – Quantifying the rate of equilibration

For each HF or LF that increases or decreases exponentially, the rate was quantified using the fit in eq. (2),

$$\langle\Delta\rangle = a \cdot \exp(-c\alpha), \tag{2}$$

where a is the asymptotic value, b is the pre-exponential factor and c is the rate constant. The range was $20° \leq \alpha \leq 120°$, consistent with the experimental fits from refs. [1, 2].

The asymptotic values and rate constants for the COMD data with and without GEMINI for the case where Z_L was fixed are shown in the left and right panels of fig. 6, respectively. The coloring and fill is consistent with fig. 5 (left). For the COMD results without GEMINI, there is no even-odd staggering present. Instead, $\langle\Delta_{asym,L}\rangle$ rises as the charge increases, with the exception of $Z_L = 3$. After GEMINI is applied, the odd-even staggering appears. However, $\langle\Delta_{asym,L}\rangle$ is lower than the experimental values. For the rate constant ($k_L(Z_L)$), the values are consistent within error bars. The experimental rate constants are on average larger than the experimental ones.

The rate constants for the combined systems (κ), as shown in fig. 5 (left and right), were determined and are shown in fig. 7. For the HF, only the AMD and experimental results were fit. Better agreement is seen between the soft interaction and the experimental results. For the LF, the rate constants are shown for AMD without GEMINI, COMD with and without GEMINI and the experimental results. All of the rate constants are significantly greater than the experimental value. An ordering is also seen where the soft interaction for both the AMD and COMD has the smallest equilibration

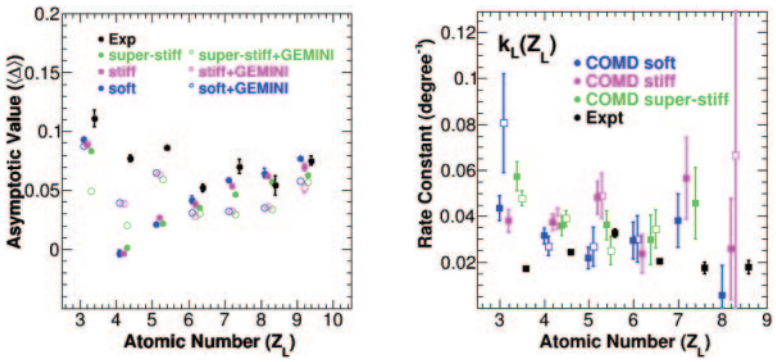

Fig. 6. – In the left panel, the asymptotic values for the COMD results with and without GEMINI as a function of the charge of the Z_L. The blue points correspond to the soft interaction, the pink points are the stiff interaction and the green points are the super-stiff interaction. The black points are the experimental values. In the right panel, the corresponding rate constants to the left panel are plotted. The coloring is consistent in both panels.

rate. When GEMINI is applied, the rate constant decreases notably for the COMD soft interaction. The effect is less present for the stiff interaction, and is negligible for the sup-stiff interaction.

To understand the lack of agreement between the experimental and simulated results for the LF, the rate constants for the experiment were determined using three different selections. In the first case, all Z_H, Z_L pairings were combined and the total system was fit, as represented by the medium hue purple in the right panel of fig. 8. The rate constant extracted is referred to as κ_L and is the left-most of the experimental points shown in the left panel of fig. 8. Next, the pairings were gated based on Z_L, where Z_H had no cuts. An example is shown using light purple points in the right panel of fig. 8. Each corresponding $\langle \Delta_L \rangle$ *vs.* α plot was fit and the weighted average was calculated. The average value was referred to as $k_L(Z_L)$ and is the middle experimental point on the left panel of fig. 8. The last rate constant corresponds to the value from ref. [1]. In

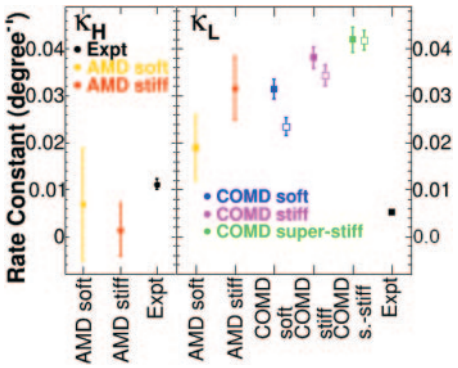

Fig. 7. – The left part is κ_H for both AMD interactions, and the experimental results. The right part is κ_L for the COMD and AMD interactions and the experimental results. The open points for the COMD κ values are with GEMINI.

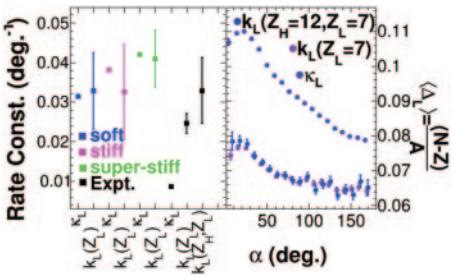

Fig. 8. – The left panel is the rate constants as a function of the pairing conditions for Z_H and $Z_L$for LF. κ is the combined system and $k_L(Z_L)$ is the average cut on Z_L. The results are compared to the experimental values. including the average rate constant from all Z_H, Z_L pairings. The right panel is the experimental Δ_L *vs.* α for all combined systems, $Z_L = 7$ and $Z_H = 14$, $Z_L = 7$.

this case, the data was sorted into Z_H, Z, L pairings and fit. The weighted average is referred to as $k_L(Z_H, Z_L)$ and correspond to the last experimental point in fig. 8. The first two selections were also applied to the COMD without GEMINI are are shown in the left panel of fig. 8.

The rate constants for the experimental data increases as the selection becomes more strict. The effect is due to mixing of yield contributions, which is most pronounced when comparing α distributions. A shift in the peak is observed for more asymmetric, larger systems. In addition, the peak is also enhanced for more asymmetric, larger systems. As a result, the combined system does not approach its asymptotic value by $\alpha = 180^\circ$ compared to the systems with at least one charge cut.

6. – Conclusions

Better agreement between the experimental and the COMD and AMD results was seen for interactions with small L-values.

For AMD, the experimental trends were reproduced for both the HF and LF. The soft interaction showed better agreement.

For COMD, the rate constant corresponding to the LF showed an ordering for results with and without GEMINI, where the soft interaction was the smallest, followed by the stiff and super-stiff interaction, respectively. In all three cases, the rate constant was overestimated relative to the experimental results. For the HF, no exponential trend was observed. An increase in the composition as a function of the rotation angle was seen for the soft interaction. The effect is lessened for the stiff interaction and is not present for the super-stiff one.

The rate constants showed better agreement after being sorted by the charge of the LF. The experimentally determined rate constant showed an increase from $\kappa \simeq 0.01$ for all Z_H, Z_L events combined to $k_L(Z_L) \simeq 0.02$ for the events sorted by Z_L. The effect is even great for events sorted by the charge of Z_H and Z_L, where the rate constant was $k_L(Z_H, Z_L) \simeq 0.03$. Hence, the evolution of the NZ equilibration in the binary decay mechanism is most accurately described when sorting by both Z_H and Z_L.

* * *

This work was supported by the Robert A. Welch Foundation Grant No. A-1266, the Department of Energy Grant No. DE-FG02-93ER40773 and the National Nuclear Security Administration Award No. NA-DE0003841.

REFERENCES

[1] Jedele A., McIntosh A. B., Hagel K., Huang M., Heilborn L., Kohley Z., May L. W., McCleskey E., Youngs M., Zarrella A. and Yennello S. J., *Phys. Rev. Lett.*, **118** (2017) 062501.
[2] Rodriguez Manso A., McIntosh A. B., Jedele A., Hagel K., Heilborn L., Kohley Z., May L. W., Zarrella A. and Yennello S. J., *Phys. Rev. C*, **95** (2017) 044604.
[3] Wuenschel S., Hagel K., Wada R., Natowitz J. B., Yennello S. J., Kohley Z., Bottosso C., May L. W., Smith W. B., Shetty D. V., Stein B. C., Soisson S. N. and Prete G., *Nucl. Instru. Methods Phys. Res. A*, **604** (2009) 578.
[4] Kohley Z., PhD Thesis, Texas A&M University (2010).
[5] Papa M., Giuliani G. and Bonasera A., *J. Comput. Phys.*, **208** (2005) 403.
[6] Akira Ono and Hisashi Horiuchi, *Prog. Part. Nucl. Phys.*, **53** (2004) 501.
[7] Harvey B., Youngs M., McIntosh A., Jedele A., Abbott A., Gauthier J., Hagel K., Hannaman A., Krieble K., Lui Y. W., McIntosh L. A., Rodriguez Manso A., Sorensen M., Tobin Z., Wada R., Zarrella A. and Yennello S., *Phys. Rev. C*, **102** (2020) 064625.
[8] Charity R. J., *Phys. Rev. C*, **58** (1998) 1073.
[9] Bocage F., Colin J., Louvel M., Auger G., Bacri Ch. O., Bellaize N., Borderie B., Bougault R., Brou R., Buchet P., Charvet J. L., Chbihi A., Cussol D., Dayras R., De Cesare N., Demeyer A., Doré D., Durand D., Frankland J. D., Galichet E., Genouin-Duhamel E., Gerlic E., Guinet D., Lautesse P., Laville J. L., Lecolley J. F., Legrain R., Le Neindre N., Lopez O., Maskay A. M., Nalpas L., Nguyen A. D., Pârlog M., Péter J., Plagnol E., Rivet M. F., Rosato E., Saint-Laurent F., Salou S., Steckmeyer J. C., Stern M., Tăbăcaru G., Tamain B., Tirel O., Tassan-Got L., Vient E., Vigilante M., Volant C., Wieleczko J. P., Le Brun C., Genoux-Lubain A., Rudolf G. and Stuttgé L., *Nucl. Phys. A*, **676** (2000) 391.
[10] Colin J., Cussol D., Normand J., Bellaize N., Bougault R., Buta A. M., Durand D., Lopez O., Manduci L., Marie J., Steckmeyer J. C., Tamain B., Van Lauwe A., Vient E., Borderie B., Lavaud F., Le Neindre N., Pawłowski P., Plagnol E., Rivet M. F., Bouriquet B., Chbihi A., Frankland J. D., Guinet D., Guiot B., Hudan S., Wieleczko J. P., Charvet J. L., Dayras R., Galichet E., Lautesse P., Nalpas L., Pârlog M., Rosato E., Roy R., Vigilante M. and Volant C., *Phys. Rev. C*, **67** (2003) 064603.
[11] Hudan S., McIntosh A. B., de Souza R. T., Bianchin S., Black J., Chbihi A., Famiano M., Frégeau M. O., Gauthier J., Mercier D., Moisan J., Metelko C. J., Roy R., Schwarz C., Trautmann W. and Yanez R., *Phys. Rev. C*, **86** (2012) 021603.